Pharmacological Research 216 (2025) 107767

Contents lists available at ScienceDirect

Pharmacological Research

journal homepage: www.elsevier.com/locate/yphrs

Age-linked DNA methylation and gene expression patterns in parameningeal head and neck alveolar rhabdomyosarcoma reveal CDK9 as a promising therapeutic target

Sara Patrizi [a,*], Silvia Vallese [b], Sabina Barresi [b], Matteo Cassandri [a], Isabella Giovannoni [b], Lucia Pedace [a], Luana Abballe [a], Flavia Vinciarelli [a], Celeste Antonacci [a], Alessandra Stracuzzi [b], Barbara Mancini [b], Ida Russo [a], Angela Di Giannatale [a], Rossella Rota [a], Rita Alaggio [b,c], Franco Locatelli [a,d], Giuseppe Maria Milano [a], Evelina Miele [a,*]

[a] Onco-Haematology, Cell and Gene Therapy, Bambino Gesù Children's Hospital, IRCCS, Rome 00165, Italy
[b] Pathology Unit, Bambino Gesù Children's Hospital, IRCCS, Rome 00165, Italy
[c] Department of Medical-Surgical Sciences and Biotechnologies, Sapienza University of Rome, Rome 00185, Italy
[d] Department of Life Sciences and Public Health, Catholic University of the Sacred Heart, Rome 00168, Italy

ARTICLE INFO

Keywords:
Alveolar Rhabdomyosarcoma
DNA methylation
Transcriptome sequencing, Targeted therapies, CDK9

ABSTRACT

Background: Alveolar rhabdomyosarcoma (ARMS) primarily affects children in the first decade of life, but it can also occur during adolescence, typically with a more favorable prognosis. This study aimed to explore differences in DNA methylation (DNAm) and gene expression profiles that may account for the worse prognosis in younger patients; and to investigate possible new therapeutic targets.

Methods: We conducted whole-genome DNAm and transcriptome analyses on 10 parameningeal head and neck ARMS patients, including 4 patients under 1 year old and 6 over 10 years old. Among the differentially expressed genes, we focused on actionable therapeutic targets and confirmed their protein expression levels by immunohistochemistry. We validated the biological relevance of molecules of interest through functional experiments on rhabdomyosarcoma cell lines.

Results: DNAm profiles did not significantly differ across age groups, while gene expression was the primary driver of observed differences. Several enriched pathways characterized younger patients with respect to older ones, including FAS, Integrin, PI3 kinase, and p53 by glucose deprivation. Among actionable molecules, cyclin dependent kinase 9 (CDK9) emerged as a promising therapy target, highly expressed in younger patients. Of note, CDK9 inhibitors specifically inhibit cell growth in bi- and three-dimensional ARMS cellular models, both as a monotherapy and in combination with BRD4 inhibitors.

Abbreviations: ARMS, Alveolar Rhabdomyosarcoma; DNAm, DNA methylation; CDK9, cyclin dependent kinase 9; 2D, bidimensional; 3D, three-dimensional; RMS, Rhabdomyosarcoma; ERMS, Embryonal Rhabdomyosarcoma; SsRMS, Spindle cell and sclerosing RMS; *PAX3*, Paired Box 3; *PAX7*, Paired Box 7; *FOXO1*, Forkhead Box O1; FP-RMS, Fusion Positive Rhabdomyosarcoma; FFPE, formalin-fixed and paraffin-embedded; MRI, Magnetic Resonance Imaging; MyoD1, myogenic differentiation antigen 1; CNV, Copy Number Variation; PCA, Principal Component Analysis; DMRs, Differentially Methylated Regions; T-SNE, t-distributed stochastic neighbor embedding; BMIQ, Beta MIxture Quantile dilation; VST, Variance Stabilizing Transformation; UCSC, University of California Santa Cruz; GEO, Gene Expression Omnibus; DEGs, Differentially Expressed Genes; GDSC, Genomics of Drug Sensitivity in Cancer; EGFR, Epidermal growth factor receptor; MTOR, Mammalian target of rapamycin; P-mTOR, phosphorylated mTOR; AP2beta, activating enhancer binding protein 2 beta; P-STAT3, phosphorylated signal transducer and activator of transcription 3; ANOVA, Analysis Of Variance; CRISPR, clustered regularly interspaced short palindromic repeats; ATCC, American Type Culture Collection; DMEM, Dulbecco's Modified Eagle Medium; FBS, fetal bovine serum; DMSO, Dimethyl Sulfoxide; PI, Propidium Iodide; RIPA, radio immunoprecipitation; EDTA, Ethylenediaminetetraacetic acid; SDS, Sodium dodecyl sulfate; BCA assay, bicinchoninic acid assay; TBS, Tris-buffered saline; GAPDH, glyceraldehyde-3-phosphate dehydrogenase; RT-qPCR, Real-time reverse transcription-quantitative Polymerase Chain Reaction; ALK, anaplastic lymphoma kinase; CT, chemotherapy; RT, radiation therapy; BVZ, bevacizumab; FN-RMS, Fusion, Negative Rhabdomyosarcoma; P3F, PAX3-FOXO1 chimeric protein; IC50, Half-maximal inhibitory concentration; BRD4, Bromodomain Containing 4; WB, Western Blot.

* Corresponding authors.
E-mail addresses: sara.patrizi@opbg.net (S. Patrizi), evelina.miele@opbg.net (E. Miele).

https://doi.org/10.1016/j.phrs.2025.107767
Received 3 April 2025; Received in revised form 7 May 2025; Accepted 7 May 2025
Available online 9 May 2025

Conclusion: Despite the small sample size, these findings suggest potential age-related molecular mechanisms and highlight candidate genes for further investigation as novel therapeutic targets. Notably, we identified CDK9 as a promising target, warranting further exploration in the context of ARMS treatment.

1. Introduction

Rhabdomyosarcoma (RMS) accounts for about 7 % of all childhood tumors and is the most common soft tissue sarcoma in children [1]. RMS can occur at any age, with 1–2 % of cases being congenital and 5–10 % diagnosed during the first year of life [2]. Incidence peaks at 2–6 years and in adolescence (14–18 years) [3]. Infants with RMS often face worse outcomes, potentially due to less intensive treatment, despite similar clinical and histologic profiles to older patients [4]. In fact, therapeutic options for ARMS patients younger than 1 year are limited by concerns for chemotherapy toxicity [5] and late effects of radiation therapy [4].

RMS is currently classified into subtypes with distinct morphological, genetic and epigenetic features: embryonal RMS (ERMS), alveolar RMS (ARMS), pleomorphic, and spindle cell and sclerosing RMS (ssRMS) [6].

ARMS is defined by chromosomal fusions involving *PAX3* (Paired box 3) or *PAX7* (Paired box 7) and *FOXO1* (Forkhead Box O1); hence its alternative definition of Fusion Positive (FP)-RMS. ARMS exhibits the least differentiated morphology among the RMS subtypes and displays aggressive metastatic behavior in up to 30 % of cases [7]. Head and neck parameningeal location of ARMS is associated with a worse prognosis in pediatric population [8]. Consistent with findings across RMS subtypes, ARMS prognosis is particularly poor in infants, with a 5-year event-free survival of 22 % [9]. On the other hand, older age has been linked to a lower disease-specific survival rate in ARMS patients [10].

This study examines ARMS cases localized to parameningeal head and neck regions in infants under 1 year old and in patients over 10 years old at the time of diagnosis, treated at our institution. Our aim is to verify the effect of age on prognosis in a population with a homogenously unfavorable location, and to identify age-associated differences in DNA methylation and gene expression that could point to novel therapeutic targets. To our knowledge, this is the first study to investigate age-related differences in ARMS on a -omic scale.

2. Methods

2.1. Case selection

For this study, we selected patients affected by parameningeal head and neck ARMS, diagnosed between March 2012 and July 2023 at Bambino Gesù Children's Hospital (Rome, Italy). Patients were categorized into two age groups: Group A (diagnosed before 1 year of age) and Group B (diagnosed after 10 years of age). We selected these age cutoffs based on several observations from the literature, reporting worse outcomes for patients under 1 year [9,11–13] or over 10 years of age [4,14]. Specimens for the analysis were retrieved from formalin-fixed and paraffin-embedded (FFPE). Tumor site identification was based on Magnetic Resonance Imaging (MRI) images and histological data, including hematoxylin-eosin and immunohistochemistry for ARMS markers (Desmin, Myogenin, and myogenic differentiation antigen 1 -MyoD1) and proliferative index (Ki67). Diagnosis was confirmed after fusion identification, as described below, with the exception of case #5 for which fusion was assessed by RT-PCR as previously described [15].

2.2. DNA methylation profiling

We extracted DNA according to MagPurix FFPE DNA Extraction Kit (Resnova) for automatic extraction of genomic DNA. Starting from 250 ng of DNA extracted from each sample, we performed bisulfite-conversion with EZ DNA Methylation Kit (Zymo Research), restoring with Illumina HD FFPE Restoration Kit (Illumina), and then screening with Illumina Human Methylation EPIC BeadChip arrays (Illumina).

We analyzed raw BeadChip data in R environment (version 4.2.1), first by performing copy number variation (CNV) analysis of each sample using R package Conumee (https://bioconductor.org/packages/devel/bioc/vignettes/conumee/inst/doc/conumee.html) and cumulative CNV visualization by group using package GenVisR [16]. We also used functions implemented in ChAMP package (version 2.26.0) [17] for data loading with method "minfi", filtering out probes located on X or Y chromosomes, known genetic polymorphisms, or with detection p-value > 0.01. We then performed functional normalization on the raw beta values. Since Singular Value Decomposition analysis revealed no significant batch effects affecting the normalized dataset's variability, we applied no further correction.

To assess sample similarity, we performed Principal Component Analysis (PCA) using the 1000 beta methylation values with highest variance. Then we computed Differentially Methylated Regions (DMRs) between groups A and B using the method "DMRcate" as implemented in package ChAMP, considering an adjusted P value threshold of 0.05 for statistical significance.

We further compared DNA methylation profiles of the collected samples to well-characterized sarcoma entities from Koelsche et al. [18] to contextualize findings with t-distributed stochastic neighbor embedding (t-SNE). Specifically, we performed data loading and probe filtering as described previously, processing each array platform separately (HumanMethylation450 or EPIC). Then, we combined the raw beta values according to the probe name and genomic position and normalized the whole matrix with BMIQ (Beta MIxture Quantile dilation) method [19]. Finally, we used the 10,000 probes with highest standard deviation to compute the 1-variance weighted Pearson correlation between the samples, then used this correlation matrix to compute the distance matrix that became the input of Rtsne function from Rtsne package (https://CRAN.R-project.org/package=Rtsne).

We also used the normalized DNA methylation data to predict the mitotic rate of tumor samples with the EpiTOC clock [20].

2.3. Gene expression profiling

We extracted RNA following ReliaPrep™ FFPE Total RNA kit (Promega) and prepared the library for sequencing using the SureSelect XT HS RNA according to manufacturer recommendations (Agilent Technologies). We verified the quality and quantity of RNA samples with Agilent 2200 Tapestation system (Agilent Technologies), and then performed total RNA sequencing on Illumina platform NEXTSEQ550.

To identify potential fusion transcripts, raw sequencing reads were preprocessed using Fastp [21] to remove low-quality reads and adapter sequences. The cleaned reads were then aligned to the human reference genome (UCSC build 38) using the STAR algorithm (v.2.5.3a) [22]. The resulting alignment files were analyzed using the Arriba [23] and FusionCatcher [24] pipelines.

We obtained RNA sequencing data from 9 healthy muscle samples of children of an intermediate age group (2–8 years old), previously published by Guadagnin et al. [25] from Gene Expression Omnibus (GEO), to use as a control group. We used Salmon (version 1.9.0) [26] to align reads of all samples to the hg38 reference genome and to perform transcript quantification. After importing gene counts in R using tximeta (1.14.1) [27], we normalized them with variance stabilizing transformation (VST) and performed PCA on the count value of the 1000 most variable genes.

We detected Differentially Expressed Genes (DEGs) between younger and older patients with adjusted P value lower than 0.05 using package

DEseq2 (v. 1.32.0) [28]. between groups A and B. To refine the DEG list, comparisons with a control group were performed, excluding genes also differentially expressed in these comparisons to eliminate potential artifacts and any gene that varies in expression in different stages of muscle growth. We explored the biological implications of the DEGs through a statistical overrepresentation test in PANTHER pathway analysis platform (https://pantherdb.org/).

To identify actionable therapeutic targets for ARMS patients, DEGs were also queried against the Genomics of Drug Sensitivity in Cancer (GDSC) database (https://www.cancerrxgene.org/).

2.4. Immunohistochemistry

We performed immunohistochemical staining to verify the protein expression of selected target genes, using the corresponding antibodies when available. For genes without available antibodies, a "proxy" gene involved in the same pathway according to the literature was used for validation.

We used 2 μm thick sections of formalin-fixed, paraffin-embedded tissue samples. The Dako Omnis platform (Agilent) was utilized for the application of the following antibodies: EGFR (Epidermal growth factor receptor, Agilent, clone E29, ready to use), desmin (Dako, clone D33, ready to use), myogenin (Dako, clone F5D, ready to use), MyoD1 (Cell Marque, clone EP212, dilution 1:50), BCL2 (Dako, clone 124, ready to use), mTOR (Mammalian target of rapamycin, Cell Signaling, clone 7C10, dilution 1:50), p-mTOR (phosphorylated mTOR, Cell Signaling, clone Ser2448 49F9, dilution 1:100), AP2beta (activating enhancer binding protein 2 beta, Santa Cruz Biotechnology, INC, clone E-8, dilution 1:100), p-STAT3 (phosphorilated signal transducer and activator of transcription 3, Cell Signaling, clone D3A7, dilution 1:250) and CDK9 (Cell Signaling, clone C12F7, dilution 1:100), following established guidelines.

The immunohistochemical expression was assessed quantitatively by determining the percentage of tumor cells exhibiting positivity.

We developed a scoring system based on the percentage of tumor cells exhibiting positivity: 0 = negative; 1 = expression in 1–25 % of cells; 2 = expression in 26–75 % of cells; 3 = expression in > 75 % of cells.

2.5. Public datasets analysis

Affymetrix profiling data from patients' public datasets (E-TABM-1202) and normal skeletal muscle samples [29] were normalized and polished using the robust multiarray average in RMAexpress. We selected a representative probeset for CDK9 expression (203198_at) and plotted expression levels for each patient subgroup and skeletal muscle in prism 10.1.1. We used One-way analysis of variance (ANOVA) to determine statistical significance. CRISPR data for a panel of RMS cell lines were downloaded from DepMap portal (https://depmap.org/portal/), using CRISPR database (Public 24Q4, 13 RMS cell lines) and plotted with Prism 10.1.1. We reported perturbation effects as Chronos score.

2.6. Cell lines

RH30 cell line was obtained from American Type Culture Collection (ATCC) while RH4 cells were provided by P. Houghton and SCMC by J. Khan. All RMS cells were cultured in Dulbecco's Modified Eagle Medium (DMEM) high-glucose (Invitrogen) supplemented with 10 % fetal bovine serum (FBS), 1 % of an L-glutamine solution and 1 % of a penicillin-streptomycin solution and at 37 °C in a humidified atmosphere of 5 % CO_2/95 % air and regularly checked for mycoplasma contamination.

2.7. Cell proliferation assay and drug treatment

1.5×10^3 RH30, RH4 and SCMC cells were seeded on 384-well plates in complete growth medium and were treated with decreasing doses of NVP-2 (10 μM-0.06 nM) or with DMSO after 24 h. Cell confluences were recorded by Celigo Image Cytometer (Nexcelom Bioscience) and half maximal inhibitory concentration (IC50) values were calculated 72 h post treatment by using the GraphPad Prism version 10.1.1. For proliferation experiments, 1.5×10^3 RH30 and RH4 cells were seeded on 384-well plates and, after 24 h (t0), media containing Dimethyl Sulfoxide (DMSO) or NVP-2 at the selected concentrations were added. Cell confluence was quantified under phase contrast every 24 h, until 72 h posttreatment using Celigo Image Cytometer (Nexcelom Bioscience). Results of dose-response curves are expressed as the mean of 3 independent experiments ± standard error of mean. Results of growth curve analysis represent the mean of 3 independent experiments ± standard deviation. Statistical significance was assessed with Student's two-tailed *t*-test.

2.8. Spheroid generation and image acquisition

For three-dimensional (3D) tumor spheroids assessment, we seeded RH4 cells in 100 μl of complete growth media on 96 Ultra-Low Attachment plates (ULA, #7007, CORNING) to obtain tumor spheroids of 300 μm diameter in 96 h. After 72 h of drug treatments, we performed Calcein AM (1 mM final concentration), Propidium Iodide (PI, 1 mg/ml final concentration) and Hoechst (1:10000) staining and acquired images by Celigo image cytometer (Nexcelom Bioscience).

2.9. Transient RNA interference

RH4 Cells were transfected with 100 nM (final concentration) siRNAs against human CDK9 (5'-TGATTGAGATTTGTCGAACCA-3') or a non-targeting siRNA as control (SIC001) (Sigma, St Louis, MO, USA) using Oligofectamine (Invitrogen, Carlsbad, CA), according to the manufacturer's recommendations. Twenty-four hours later, the medium was replaced with fresh complete growth medium and transfected cells were harvested at 48 h post-transfection for subsequent analysis.

2.10. Western blot

We performed Western blotting on whole-cell lysates by homogenizing cells in RIPA lysis buffer (50 mM Tris pH 7.4, 150 mM NaCl, 1 % Triton X-100, 1 mM EDTA, 1 % sodium deoxycholate, 0.1 % Sodium dodecyl sulfate - SDS), containing the protease inhibitor cocktail (Sigma), NaF 1 mM, Na3VO4 1 mM and PMSF 1 mM. Lysates were incubated on ice for 30 minutes (min) and centrifuged at 12,000xg for 20 min at 4°C. Supernatants were used as total lysates. We estimated protein concentrations with the BCA protein assay (bicinchoninic acid assay, Pierce), according to the manufacturer's protocol. The proteins (40 μg) were boiled in reducing SDS sample buffer (200 mM Tris–HCl pH 6.8, 40 % glycerol, 20 % β-mercaptoetanol, 4 % SDS, and bromophenol blue), and run on 8 % SDS-polyacrylamide gels. Then, the proteins were transferred to Hybond ECL membranes (Amersham, GE HEALTHCARE BioScience Corporate Piscataway). Membranes were blocked in 5 % non-fat dried milk in Tris-buffered saline (TBS) for 1 h and incubated overnight (ON) with the appropriate primary antibody at 4°C. After incubation, membranes were washed in TBS and incubated with the appropriate secondary antibody for 1 h at room temperature. Detection was performed by Pierce™ ECL Western Blotting Substrate (Thermo Scientific) or Western Lightning ECL Pro (PerkinElmer,). Antibody against FOXO1 (#2880) and GAPDH (glyceraldehyde-3-phosphate dehydrogenase, #2118) was from Cell Signaling Technology, MYCN was from Santa Cruz Biotechnology (B8.4.B; sc-53993) and Vinculin antibody was from Sigma-Aldrich (V9131). We used all antibodies in accordance with manufacturer's instructions.

2.11. Real-time reverse transcription-quantitative PCR (RT-qPCR)

We extracted total RNA from cells using TRIzol (Invitrogen) according to manufacturer's protocol. We performed reverse transcription with Improm-II Reverse Transcription System (A3800, Promega), then measured gene expression levels for relative quantification with qRT-PCR on Applied Biosystems 7900HT Fast RealTime PCR System, using TaqMan gene assay (Applied Biosystems, Life Technologies, Carlsbad, CA, USA) for human ALK (Hs00608284_m1) and CDK9 (Hs00977896_g1). We normalized values according to the human GAPDH (Hs99999905_m1) mRNA levels and calculated the expression fold change by the 2- ΔΔCt method for each reference gene. was We performed at least two independent amplifications for each probe, in triplicate. Results represent the mean of at least 2 independent experiments ± standard deviation. Statistical significance was assessed with Student's two-tailed *t*-test.

3. Results

We selected a cohort of 10 patients affected by head and neck ARMS (clinical characteristics are summarized in Table 1). All patients harbored the pathognomonic *PAX3::FOXO1* fusion translocation, except for patient #10, who presented *PAX7::FOXO1* fusion. The cohort included six male and four female patients. Four patients received their diagnosis before the age of one (Group A), while the remaining six were diagnosed after the age of 10 (Group B). At the latest follow up, 6 patients (3 from Group A and 3 from Group B) had died, while 4 patients (1 from Group A and 3 from Group B) were alive. The outcomes varied significantly, ranging from patient #3, who died 3 months after diagnosis, to patient #8, who remained alive and well after 85 months of follow-up. Notably, all patients in Group A had metastases at the time of diagnosis, whereas none of the patients in Group B had metastases. All patients received chemotherapy; in addition, Bevacizumab was administered to 2/4 patients in Group A, and radiation therapy (RT) in 1/4 Group A (brachytherapy) and 4/6 Group B patients (external beam RT).

Representative MR images at diagnosis are shown in Fig. 1A. All tumors presented as heterogeneous masses, with contrast enhancement and signal restriction, indicative of highly cellular components. Tumors in Group A appeared bulkier. Intracranial and bone involvement was evident for patients #3 and #5. All tumors displayed parameningeal involvement.

Hematoxylin-eosin staining (Fig. 1B) revealed a homogenous morphology. The tumors were composed of round cells with a pale eosinophilic cytoplasm and rounded nuclei, with a solid and/or pseudoalveolar pattern of growth. Desmin, Myogenin, and MyoD1 were diffusely positive in all samples (examples from patient #3 are shown in Fig. 1C), as well as AP2beta in the tested cases. Ki67 was high in tested cases.

Analysis of DNA methylation data revealed partial separation between the two age groups along the first principal component (horizontal axis, PC1), aligning with age at tumor onset (Fig. 2A). However, differential methylation analysis identified no significant DMRs between the groups. In t-SNE analysis, all samples clustered closely with reference ARMS cases, confirming high similarity regardless of age group (Fig. 2B). CNV analysis revealed predominantly flat profiles in Group A patients (Fig. 2C and Supplementary Figure 1), while Group B cases displayed a higher frequency of complex genomic alterations (Fig. 2D and Supplementary Figure 1).

We also estimated the mitotic ages of ARMS samples based on their raw DNAm data. We observed a positive correlation (score 0.7, R [2]= 0.49) between the number of CNVs and mitotic rate (Fig. 2E), suggesting that a higher proliferation rate could be responsible for an accumulation of genomic alterations. In accordance, we observed a negative correlation (score –0.6, R^2= 0.42) between survival and mitotic rate (Fig. 2F).

We analyzed RNA sequencing for 9 of the 10 ARMS patients (excluding patient #5 due to low RNA quality) and 9 control samples of pediatric healthy muscle from a public database [25]. PCA of the 1000 most variable genes revealed a strong separation between ARMS and control samples along PC1, with partial overlap between the two ARMS age groups (Fig. 3A). The differential gene expression analysis workflow is summarized in Fig. 3B. A total of 8361 genes were differentially expressed between Group A and Group B. Compared to controls, 13968 genes were significantly differentially expressed in younger patients, and 18384 in older patients. Of these, 11938 genes were shared between both age groups when compared to controls, leaving 5601 transcripts differentially expressed uniquely between Group A and Group B. Specifically, 625 transcripts were more expressed in Group A. The most enriched pathways among these genes included FAS signaling pathway (P00020), Integrin signaling pathway (P00034), mRNA splicing (P00058), PI3 kinase pathway (P00048), p53 pathway by glucose deprivation (P04397). The remaining 4976 genes were more expressed in Group B. Pathway enrichment results on this gene group yielded the following top hits: Blood coagulation (P00011), 5-Hydroxytryptamine biosynthesis (P04371), Heterotrimeric G-protein signaling pathway-Gi alpha and Gs alpha mediated pathway (P00026), Nicotine degradation (P05914), Arginine biosynthesis (P02728) (Fig. 3C and Supplementary

Table 1
Demographic and clinical characteristics of head and neck ARMS patients included in the study. CT=chemotherapy, RT=radiation therapy, BVZ= bevacizumab.

Sample ID	Sex	Age at diagnosis (years)	Age group	Fusion	Survival (months)	Status at last follow up	Localization	Metastases at diagnosis (yes/no - localization)	Therapy
1	M	0.67	A	*PAX3::FOXO1*	12	Dead	Right cervicofacial-mediastinal	Yes (abdomen)	BVZ + CT
2	M	0.83	A	*PAX3::FOXO1*	22	Dead	Maxillary sinus	Yes (L4 vertebra)	CT
3	F	0.5	A	*PAX3::FOXO1*	3	Dead	Right orbit	Yes (abdomen)	BVZ + CT
4	F	0.92	A	*PAX3::FOXO1*	36	Alive	Left jaw	Yes (lymph nodes)	CT + RT
5	F	16	B	*PAX3::FOXO1*	10	Dead	Right sub-mandibular region	No	CT + RT
6	M	15	B	*PAX3::FOXO1*	29	Dead	Left nasal fossa	No	CT
7	M	14	B	*PAX3::FOXO1*	19	Dead	Anterior cranial fossa	No	CT + RT
8	M	15	B	*PAX3::FOXO1*	85	Alive	Right nasal fossa	No	CT + RT
9	M	17	B	*PAX3::FOXO1*	25	Alive	Right maxillary sinus	No	CT + RT
10	F	10	B	*PAX7::FOXO1*	15	Alive	Parotid and temporal region	No	CT

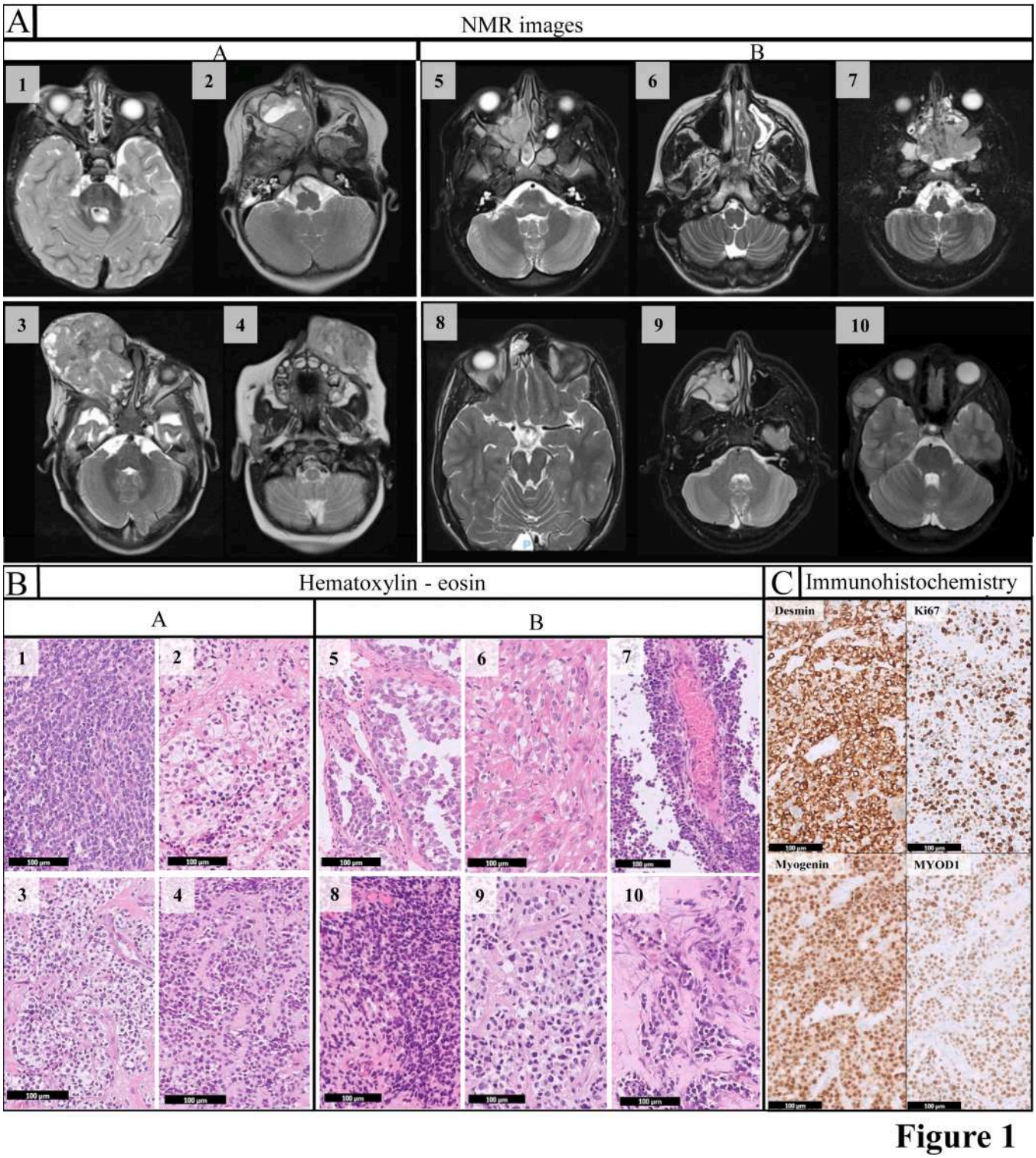

Fig. 1. Radiological and histological characterization. A –MRI images of ARMS at diagnosis. B – Hematoxylin and eosin staining of ARMS tissue from each patient. Scale bar: 100 μm. C – Representative immunohistochemistry (IHC) staining for the proteins desmin, Ki67, myogenin, and MYOD1 in ARMS patient (#3).

Table 1).

Among the differentially expressed genes, 22 were included as drug targets in the GDSC database. Six transcripts (*CAPN1*, *KDM3A*, *CDK9*, *PARP1*, *AKT2*, *AKT1*) were more expressed in Group A, while the remaining 16 (*ROS1*, *BRDT*, *ESR1*, *ESR2*, *PIM2*, *RAC2*, *BTK*, *TEC*, *NUAK2*, *AURKC*, *EGFR*, *CDK5*, *NTRK2*, *KIT*, *LRRK2*, *PLK2*) were more expressed in Group B.

We assessed the protein expression of EGFR, BCL2, mTOR and p-mTOR (downstream of AKT1), p-STAT3 (downstream of KDM3A), and CDK9. Patient #3 was excluded from the analysis due to insufficient material. Quantitative staining scores for each protein and patient are summarized in Fig. 4A. In Group A, all evaluated patients (3) exhibited a score of 0 for EGFR, a score of 3 for mTOR and CDK9; while BCL2 was positive in 2 patients (scores 1 and 2). p-mTOR and p-STAT3 were positive in one patient each, with scores of 2 and 1, respectively. In Group B, EGFR was positive in 1/6 patients (score 1); BCL2 in 5/6 (score

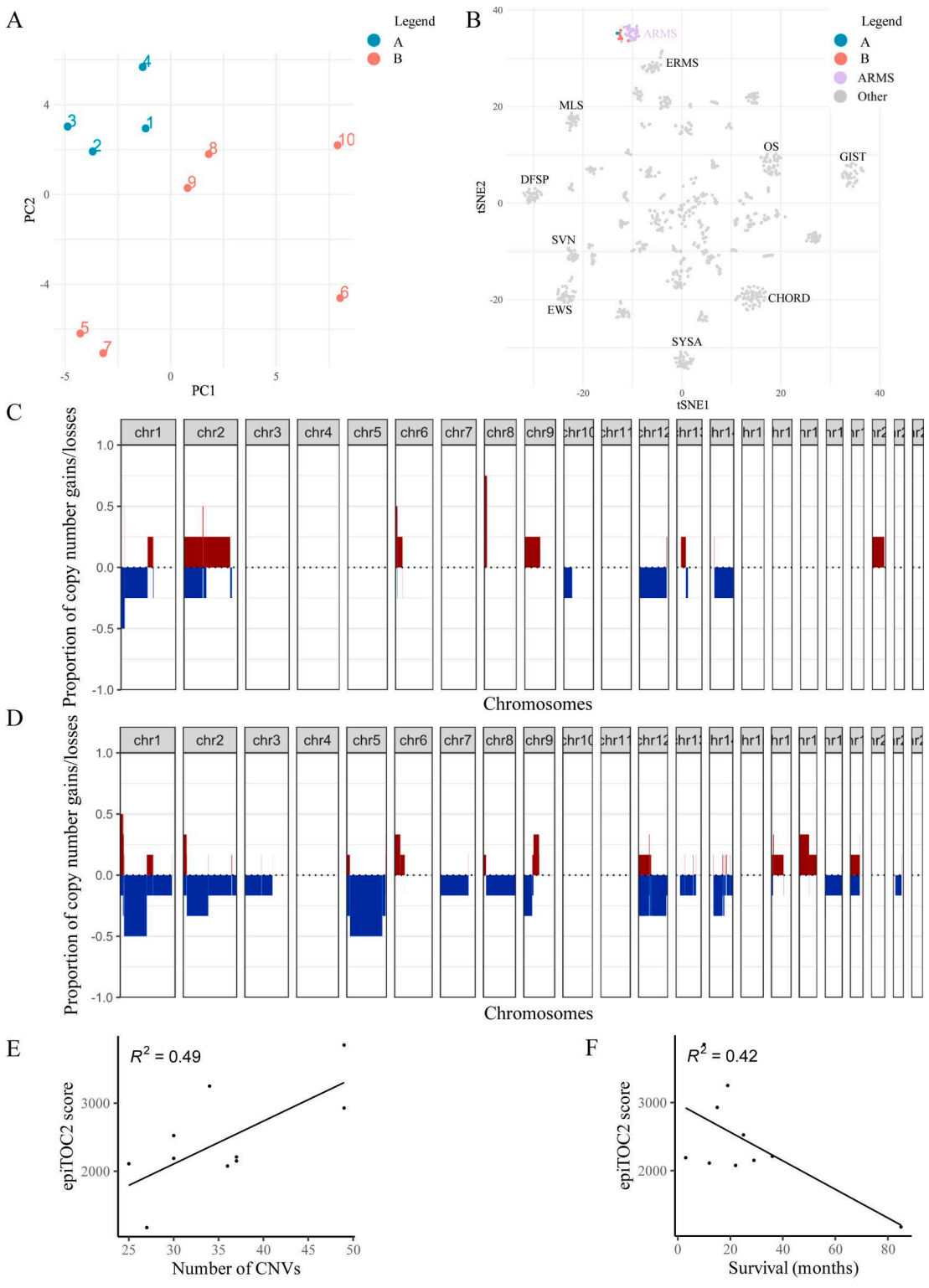

Figure 2

Fig. 2. Whole-genome DNA methylation analysis. A – Principal Component Analysis (PCA) of the beta values for the 1000 most variable probes in the whole genome methylation data. Patients aged > 10 years are represented in pink, while patients aged < 1 year are shown in aqua. B – t-Distributed Stochastic Neighbor Embedding (tSNE) of DNA methylation data, including the ARMS samples recruited for this study and other sarcomas with various histologies as described by Koelsche et al. Patients aged < 1 year (A) are shown in aqua, patients aged > 10 years (B) in pink, reference ARMS samples in lilac, and other sarcoma entities in grey. C and D – Cumulative copy number variation (CNV) plots showing the proportion of copy number gains (red) and losses (blue) across all chromosomes in ARMS group A (C) and ARMS group B (D), respectively. E and F – Linear regression analysis between the epiTOC2 mitotic clock score (Y-axis) and (E) the number of CNVs on the X-axis, and (F) survival in months on the X-axis.

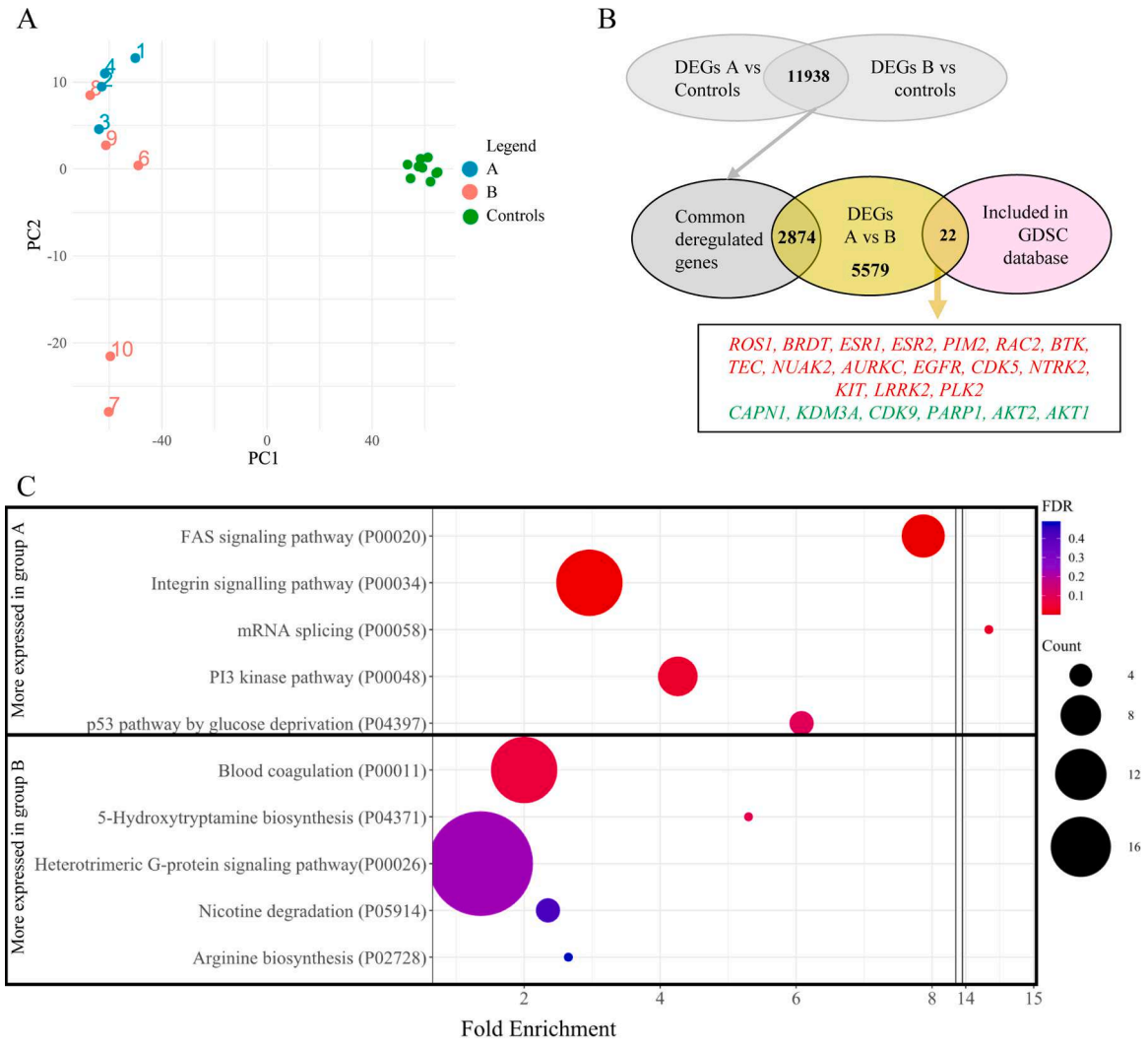

Figure 3

Fig. 3. Gene expression analysis. A – PCA of the counts for the 1000 most variable genes across the whole transcriptome RNA sequencing data. Patients aged < 1 year (A) are represented in aqua, patients aged > 10 years (B) in pink, and control tissues in green. B – Schematic representation of the gene selection process. Genes in red are more highly expressed in patients over 10 years of age (B), while genes in green are more highly expressed in patients under 1 year of age (A). C – Plot of the top 5 enriched Panther pathways for genes more highly expressed in group A (top) or group B (bottom). For each enriched pathway (Y-axis), the dot position on the X-axis represents the fold enrichment relative to the expected value. Dot color indicates the adjusted p-value, and dot size corresponds to the number of genes included in the pathway.

1 in 3 patients and 2 in 2). mTOR was expressed in 6/6 patients (score 3), p-mTOR was highly expressed (score 3) in 3/6 patients and weakly in 1/6 (score 1), while p-STAT3 was positive in 2/6 (score 1). CDK9 was expressed in all Group B patients with scores of 3 in 4/6, 2 in 1/6, and 1 in 1/6. Representative images for one case from each age group are shown in Fig. 4B. Linear regression analysis showed a modest but positive correlation between the RNA VST-normalized read counts and IHC quantitative score of EGFR (R2 =0.22, Fig. 4C) and CDK9 (R2 =0.26, Fig. 4D).

CDK9 is emerging as a promising therapeutic target in pediatric sarcomas [30]. To further investigate its role in ARMS, we first analyzed a public Affymetrix dataset to assess its expression in patients. Our analysis confirmed that CDK9 is significantly overexpressed in both Fusion negative (FN)-RMS and FP-RMS compared to normal skeletal muscle tissue (Fig. 5A). Additionally, CRISPR/Cas9 knockout (KO) data from the DepMap portal (Achilles project, https://depmap.org/portal/achilles) demonstrated that both FP-RMS and FN-RMS cell lines are highly dependent on CDK9 expression for survival (Chronos score < −1) (Fig. 5B). These findings suggest that CDK9 inhibition could be a promising strategy for suppressing RMS tumor growth.

To evaluate the efficacy of CDK9 inhibition, we conducted dose-response experiments on ARMS (FP-RMS) cell lines (RH4, RH30 and SCMC), using the selective CDK9 inhibitor NVP-2. The results showed that all the cell lines exhibited extremely low IC50 values (RH4: 4.6 nM, RH30: 2.9 nM, SCMC: 1.7 nM) (Fig. 5C). Additionally, a 72-hour growth assay in RH30 and RH4 cells demonstrated a significant reduction in proliferation following NVP-2 treatment compared to DMSO-treated controls, with inhibitory effects becoming evident as early as 24 hours post-treatment (Fig. 5D). We next evaluated the efficacy of NVP-2 treatment in a 3D tumor spheroid model using RH4 cells. A high dose of NVP-2 (1 μM) strongly inhibited cell growth, drastically reducing the number of live cells while inducing significant cell death. Notably, even a low dose (5 nM), which was effective in bidimensional (2D) cultures, was sufficient to suppress 3D cell proliferation (Fig. 5E).

CDK9 is a transcriptional kinase involved in regulating RNA polymerase II activity [30], and ARMS are driven by an aberrant

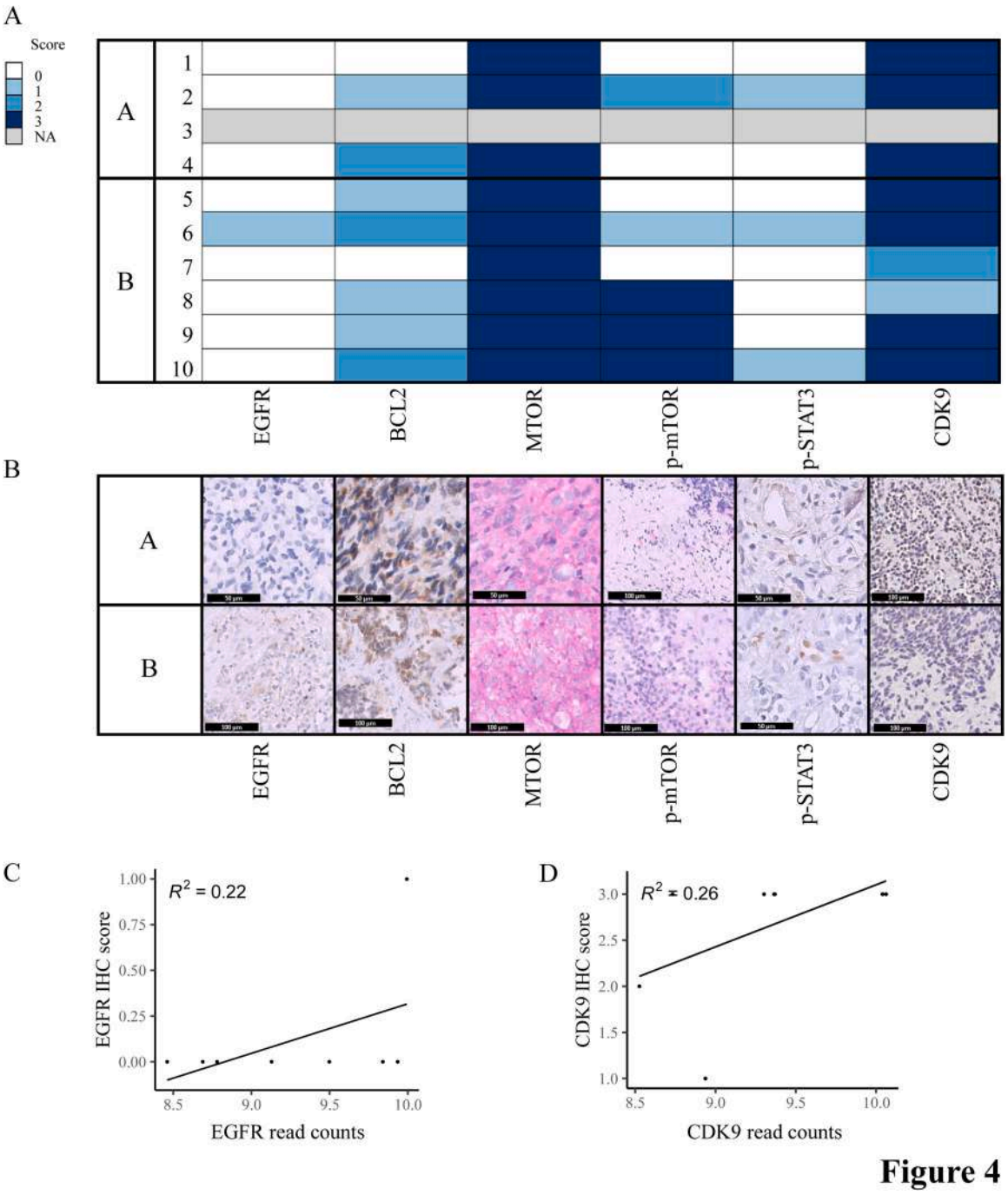

Fig. 4. Immunohistochemical validation of protein expression. A – IHC staining results for proteins of interest (EGFR, BCL2, mTOR, p-mTOR, p-STAT3, CDK9). Each square represents the quantitative score for the staining of a given protein (column) in each patient (row), with age groups indicated in horizontal boxes. Scores range from 0 (white) to 3 (dark blue). Unavailable stainings (NA) are represented by gray squares. B – Representative IHC staining images for each protein of interest across different age groups. Scale bars are either 100 μm or 50 μm, as indicated. C and D – Linear regression analysis between RNA sequencing normalized counts (X-axis) and IHC quantitative scores (Y-axis) for EGFR (C) and CDK9 (D).

transcriptional program orchestrated by a core regulatory transcription factor complex, including key components MYCN and PAX3-FOXO1 chimeric protein (P3F) [31]. To assess the impact of CDK9 inhibition on these oncogenes, we treated RH30 cells with NVP-2. Interestingly, a 6-hour treatment with 25 nM NVP-2 reduced MYCN protein levels (Fig. 5F), while a 24-hour treatment at the IC50 dose led to a decrease in P3F levels (Fig. 5G) and downregulation of its target gene *ALK* at the mRNA level (Fig. 5H).

To confirm the specificity of these effects, we silenced *CDK9* expression in RH4 cells for 48 h. Consistently, CDK9 knockdown resulted in reduced MYCN and P3F protein levels (Fig. 5I) as well as decreased *ALK* mRNA expression (Fig. 5J), reinforcing the role of CDK9 in regulating these oncogenic drivers.

P3F is a chimeric fusion transcription factor considered challenging to target directly. However, recent studies have shown that BRD4 inhibition can suppress its transcriptional activity [31]. Based on this, we investigated the combinatorial effects of JQ1 (an inhibitor of BRD4 - Bromodomain Containing 4 gene inhibitor) and NVP-2 in RH4 cells.

Interestingly, NVP-2 at its IC50 dose and JQ1 at 300 nM individually reduced cell proliferation by approximately 50 % and 30 %,

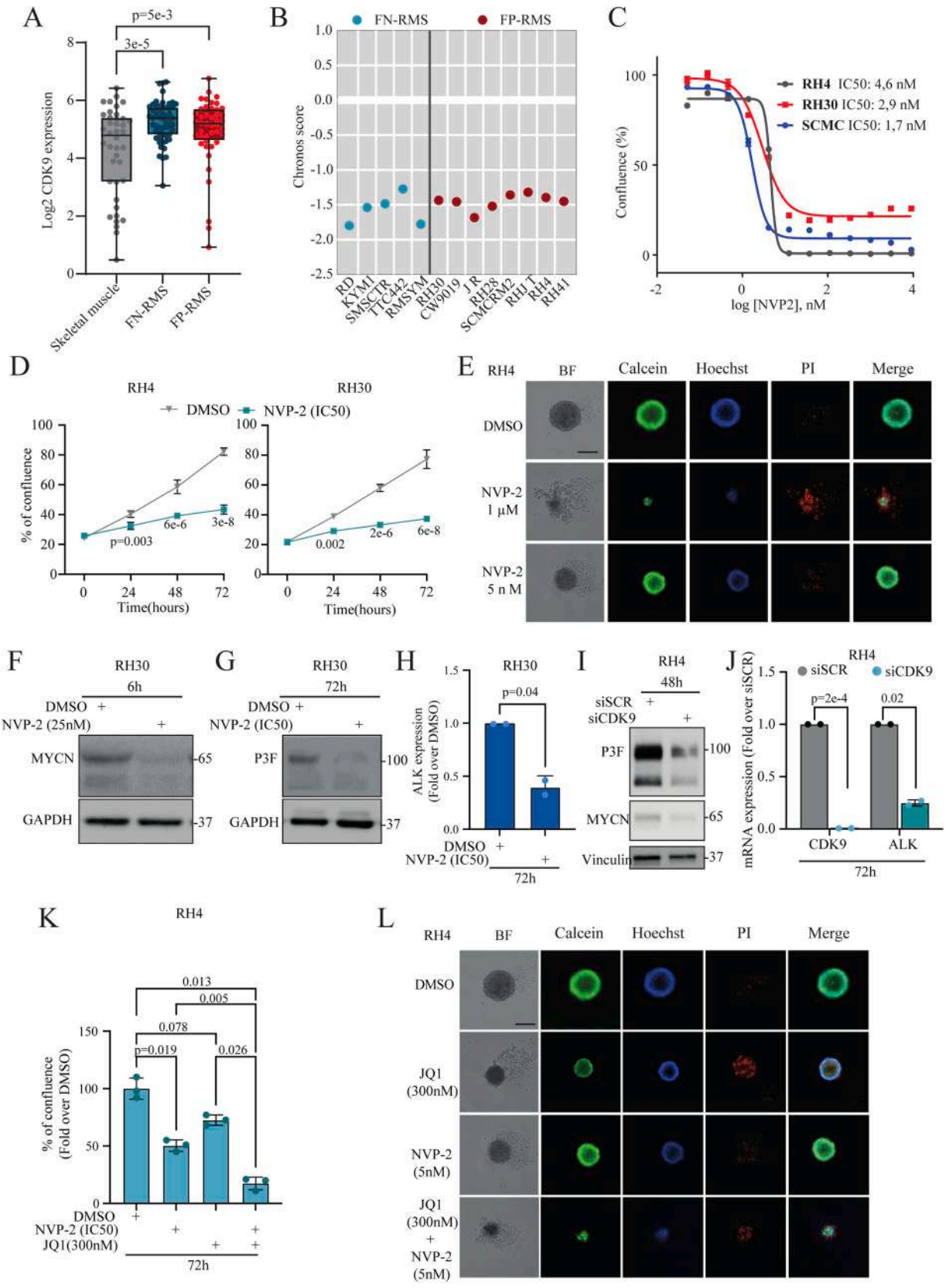

Figure 5

(caption on next page)

Fig. 5. *In vitro* validation of the role of CDK9 inhibition in ARMS cells. A – Boxplot depicting CDK9 expression among normal skeletal muscle (n = 40), FN-RMS (n = 56) and FP-RMS (n = 44). B – Dependency (Chronos score) of FN-RMS and FP-RMS cell lines from CDK9 expression (from DepMap). C - Dose-response curves of RH4, RH30 and SCMC FP-RMS cells treated with increasing concentration of NVP-2. D - Growth curve analysis of RH30 and RH4 cells treated with NVP-2 at IC50 doses reported in C. E - Representative images of RH4 tumor spheroids treated for 72 h with NVP-2 (1 μM and 5 nM), marked with Calcein (green, live cells), Propidium Iodide (PI, red, dead cells) and Hoechst (blue, all cells). Scale bars = 500 μm. F – Representative Western Blot (WB) showing MYCN protein level in RH30 cells treated with NVP-2 (25 nM) or DMSO for 6 h. G - Representative WB showing PAX3-FOXO1 (P3F) protein level in RH30 cells treated with NVP-2 (IC50) or DMSO for 72 h. H - mRNA levels (RT-qPCR) of ALK on RH30 cells treated as in G, normalized to GAPDH levels and expressed as fold increase over DMSO. I - Representative WB showing P3F and MYCN protein levels in RH4 cells transfected with either Scrambled siRNA (siSCR) or CDK9 siRNA (siCDK9) at 48 h post-transfection. J - mRNA levels (RT-qPCR) of CDK9 and ALK on RH4 cells treated as in I, normalized to GAPDH levels and expressed as fold increase over DMSO. K – Histogram depicting cell confluence of RH4 cells treated with NVP-2 (IC50) and JQ1 (BRD4 inhibitor; 300 nM) as single agents or in combination for 72 h. Mean of 2 independent experiments ± SD, Student's two-tailed *t*-test. L - Representative images of RH4 tumor spheroids treated as in K, marked with Calcein (green, live cells), Propidium Iodide (PI, red, dead cells) and Hoechst (blue, all cells). Scale bars = 500 μm.

respectively. However, their combination produced a significantly stronger effect, reducing cell growth by nearly 85 % (Fig. 5K). Furthermore, we tested this combination in a 3D RH4 tumor spheroid model, where it markedly suppressed spheroid growth and significantly decreased the number of viable cells (Fig. 5L).

Collectively, these findings provide proof of concept for the therapeutic efficacy of CDK9 inhibition in ARMS, both as a single agent and in combination with BRD4 inhibitors.

4. Discussion and conclusions

This study examined a cohort of patients with parameningeal head and neck ARMS, with the aim to investigate age-associated biological factors, that may impact clinical outcomes, and identify potential therapeutic targets to complement conventional treatments, particularly for younger patients with less favorable prognoses.

The cohort included 10 patients: 4 diagnosed during their first year of life (Group A) and 6 after 10 years of age (Group B). Male patients predominated (6 males vs. 4 females), consistent with literature on rhabdomyosarcoma [32]. The cohort was homogenous regarding driver genetic events, tumor localization and morphology, and marker expression.

Group A had higher mortality (75 %, 3/4) than Group B (50 %, 3/6), aligning with previous findings [4]. At diagnosis, Group A displayed more aggressive phenotypes, with metastatic disease in all cases. Notably, the only patient in group A that had received radiation therapy was also the one with the longest overall survival and the only one alive at the time of writing. These observations support the concept that the worse prognosis observed in infants with RMS could be, at least in part, due to the fact that radiation therapy is often omitted or limited [11].

Conversely, Group B showed more complex CNV profiles, suggesting prolonged disease duration and additional DNA alterations beyond the fusion driver. Irrespective of age, samples with a higher mitotic rate according to the epigenetic clock showed a higher number of CNVs and poorer overall survival.

DNA methylation profiles were similar across both age groups and clustered together with larger methylome reference data [18]. However, transcriptional profiling revealed significant differences between the groups.

The genes overexpressed in Group A belonged to pathways that have a known role in ARMS growth and metastasis, coherently with a more aggressive clinical behavior in this age group. Specifically, the characteristic P3F oncoprotein has been linked to an increase in the activation of the PI3 kinase pathway [33] and of glucose uptake through loss of p53 activity [34]. In ARMS cells, p53 suppression is also achieved through alternative mRNA splicing of *MDM2* and *MDM4* genes [35]. The alternative isoforms also have a direct effect in promoting invasion and metastasis. Moreover, an enrichment of proteins related to FAS and integrin signaling has been observed in exosomes derived from ARMS cell lines [36].

The genes that were more highly expressed in Group B, on the other hand, exhibited a wider range of diverse and unexpected functions. The most significantly enriched pathway among them was blood coagulation. Hypercoagulability has been observed in several pediatric cancers, including rhabdomyosarcomas [37]. Case reports of intravascular coagulation in alveolar rhabdomyosarcomas are sparse, but older age emerged as a risk factor for this condition [38], supporting our observation.

Key findings of the differential expression analysis with potential pharmacological relevance included the upregulation of AKT1, p-STAT3, and CDK9 in younger patients and EGFR in older ones. mTOR was consistently expressed across all samples, though its phosphorylation was more frequent in Group B (4/6) compared to Group A (1/3), contrary to transcriptomic data suggesting broader pathway activation.

EGFR expression was minimal and sporadic, with only one Group B case being positive, reflecting its limited potential as a robust drug target for ARMS [39]. Nevertheless, its role in tumorigenesis warrants further study in larger cohorts.

Immunohistochemical analysis showed high expression of CDK9 across the cohort, particularly in Group A. This protein is implicated in cancer metastasis, including soft tissue sarcomas [40]. Early studies of CDK9 inhibitors in sarcoma treatment have shown promise [41]. Particularly, it recently emerged as a vulnerability in Ewing Sarcoma, where CDK9 inhibition induces *EWS::FLI* downregulation, impairing its oncogenic transcriptional program [42]. As a validated drug target [30], it is being investigated in currently recruiting trials in the context of hematological malignancies [43], advanced solid tumors and lymphomas [44].

Our findings support CDK9 as a promising therapeutic target in ARMS. Analysis of public datasets confirmed its overexpression in FN-RMS and FP-RMS, with CRISPR/Cas9 screening revealing its essential role in RMS cell survival [30].

CDK9 inhibition using NVP-2 showed strong anti-proliferative effects in ARMS cell lines, with low IC50 values and significant reduction in 3D tumor spheroids. Mechanistically, NVP-2 treatment downregulated key oncogenes MYCN and P3F, along with the P3F target gene ALK, effects that were confirmed via CDK9 knockdown [31].

Given the difficulty in directly targeting P3F, we explored a combinatorial approach using the BRD4 inhibitor JQ1. This combination significantly enhanced anti-tumor effects, both in 2D cultures and 3D spheroids, demonstrating potential synergy in disrupting ARMS transcriptional regulation. These data support the recent findings in Ewing sarcoma that CDK9 interacts directly with BRD4, and that CDK9 inhibition enhances cellular sensitivity to JQ1 treatment [42].

Taken together, these results provide strong preclinical evidence for CDK9 inhibition as a viable therapeutic strategy in ARMS, both as a monotherapy and in combination with BRD4 inhibitors; mostly for the high-risk group of parameningeal head and neck infantile tumors, where radiation therapy is less applicable. In recent years, a wider application of tailored and localized radiation therapy in infants has been associated with a better overall survival [45]. While the positive clinical impact of radiation therapy is undeniable, there is still a relevant therapeutic gap, that CDK9 inhibitors could fill either when radiation therapy is not feasible or when the patients do not respond. Larger clinical studies would be needed to assess their efficacy and to elaborate specific treatment schedules.

In conclusion, our study provides a detailed molecular characterization of pediatric and infantile ARMS in the parameningeal head and neck region. Despite the small sample size, our findings indicate homogenous DNA methylation profiles across age groups but reveal distinct transcriptional profiles, including potential targetable genes such as CDK9. Further validation in larger patient cohorts and *in vivo* studies could pave the way for clinical translation of these findings. Such advancements may enable the development of novel treatment strategies aimed at improving outcomes for patients with this aggressive pediatric sarcoma, especially for those with limited therapeutic options.

CRediT authorship contribution statement

Alaggio Rita: Writing – review & editing, Supervision, Resources, Funding acquisition. **Cassandri Matteo:** Writing – review & editing, Writing – original draft, Visualization, Methodology, Investigation, Funding acquisition, Formal analysis, Conceptualization. **Locatelli Franco:** Writing – review & editing, Supervision, Resources. **Giovannoni Isabella:** Writing – review & editing, Methodology, Investigation, Formal analysis. **Milano Giuseppe Maria:** Writing – review & editing, Supervision, Resources, Funding acquisition, Conceptualization. **Pedace Lucia:** Writing – review & editing, Visualization, Methodology, Investigation, Formal analysis. **Miele Evelina:** Writing – review & editing, Writing – original draft, Supervision, Methodology, Investigation, Funding acquisition, Conceptualization. **Abballe Luana:** Writing – review & editing, Visualization, Methodology, Investigation, Formal analysis. **Vinciarelli Flavia:** Writing – review & editing, Methodology, Investigation, Formal analysis. **Antonacci Celeste:** Writing – review & editing, Methodology, Investigation, Formal analysis. **Stracuzzi Alessandra:** Writing – review & editing, Methodology, Investigation, Formal analysis. **Mancini Barbara:** Writing – review & editing, Methodology, Investigation. **Russo Ida:** Writing – review & editing, Methodology, Investigation, Formal analysis. **Patrizi Sara:** Writing – review & editing, Writing – original draft, Visualization, Methodology, Investigation, Formal analysis, Data curation. **Di Giannatale Angela:** Writing – review & editing, Methodology, Investigation, Formal analysis. **Vallese Silvia:** Writing – review & editing, Methodology, Investigation, Formal analysis. **Rota Rossella:** Writing – review & editing, Supervision, Resources, Funding acquisition, Conceptualization. **Barresi Sabina:** Writing – review & editing, Methodology, Investigation, Formal analysis.

Ethics approval and consent to participate

This study was reviewed and approved by Bambino Gesù Children's Hospital Ethical Committee (protocol number 2126_OPBG_2020, June 17, 2020; final approval received on November 22, 2020). An informed consent was obtained from all patients' parents. All procedures were carried out in accordance with the Helsinki Declaration. Human tissues were procured in line with WHO Guiding Principles on Human Cell, Tissue and Organ Transplantation. A limitation to the generalisability of the study is that it did not consider gender/sex issues.

Consent for publication

Consent for publication was obtained from the participants.

Funding

This research was supported by the Italian Ministry of Health, Ricerca Corrente (202005_ONCO_MIELE to E.M; 202005_ONCO_ALAGGIO to R.A., and 202203_FBG_MILANO.1.15 to G.M.M); Italian Ministry of Health Ricerca Finalizzata GR-2021–12374415 to M.C.; Associazione Italiana Ricerca sul Cancro (AIRC IG #10338, #15312 and #27794) to R.R.

Declaration of Competing Interest

The authors declare that they have no known competing financial interests or personal relationships that could have appeared to influence the work reported in this paper.

Acknowledgements

The authors thank Associazione il Cuore grande di Flavio for their support. Sara Patrizi and Luana Abballe have been supported by Fondazione Umberto Veronesi.

Appendix A. Supporting information

Supplementary data associated with this article can be found in the online version at doi:10.1016/j.phrs.2025.107767.

Data Availability

DNAm and RNA sequencing raw data are deposited in NCBI's Gene Expression Omnibus (GEO; Series accession number GSE289527 and GSE289529 respectively).

References

[1] E. Koscielniak, M. Morgan, J. Treuner, Soft tissue sarcoma in children: prognosis and management, Pedia Drugs 4 (1) (2002) 21–28, https://doi.org/10.2165/00128072-200204010-00003.
[2] L. Wexler, W. Crist, L. Helman, Rhabdomyosarcoma and the Undifferentiated Sarcomas, in: P.A. Pizzo, D.G. Poplack (Eds.), Principles and Practice of Pediatric Oncology, 4th Edition, Lippincott Williams & Wilkins, Philadelphia, 2022.
[3] S. Weiss, J. Goldblum, Rhabdomyosarcoma, in: S.W. Weiss, J.R. Goldblum (Eds.), Enzinger and Weiss's Soft Tissue Tumors, 4th Edition, St Louis: CV Mosby, 2001.
[4] D. Joshi, J.R. Anderson, C. Paidas, et al., Age is an independent prognostic factor in rhabdomyosarcoma: a report from the Soft Tissue Sarcoma Committee of the Children's Oncology Group, Pedia Blood Cancer 42 (1) (2004) 64–73, https://doi.org/10.1002/pbc.10441.
[5] A.H. Ragab, R. Heyn, M. Tefft, D.N. Hays, W.A. Newton Jr., M. Beltangady, Infants younger than 1 year of age with rhabdomyosarcoma, Cancer 58 (12) (1986) 2606–2610, https://doi.org/10.1002/1097-0142(19861215)58:12< 2606::AID-CNCR2820581209> 3.0.CO;2-T.
[6] E.R. Rudzinski, A. Kelsey, C. Vokuhl, et al., Pathology of childhood rhabdomyosarcoma: a consensus opinion document from the Children's Oncology Group, European Paediatric Soft Tissue Sarcoma Study Group, and the Cooperative Weichteilsarkom Studiengruppe, Pedia Blood Cancer 68 (3) (2021) e28798, https://doi.org/10.1002/pbc.28798.
[7] W.T.A. van der Graaf, D. Orbach, I.R. Judson, A. Ferrari, Soft tissue sarcomas in adolescents and young adults: a comparison with their paediatric and adult counterparts, Lancet Oncol. 18 (3) (2017) e166–e175, https://doi.org/10.1016/S1470-2045(17)30099-2.
[8] C.M. Heske, Y.Y. Chi, R. Venkatramani, et al., Survival outcomes of patients with localized FOXO1 fusion positive rhabdomyosarcoma treated on recent clinical trials: a report from the Soft Tissue Sarcoma Committee of the Children's Oncology Group, Cancer 127 (6) (2021) 946–956, https://doi.org/10.1002/cncr.33334.
[9] S. Malempati, D.A. Rodeberg, S.S. Donaldson, et al., Rhabdomyosarcoma in infants less than one year of age: a report from the Children's Oncology Group, Cancer 117 (15) (2011) 3493–3501, https://doi.org/10.1002/cncr.25887.
[10] J.C.V. Gaal, W.T. a V.D. Graaf, B. Rikhof, et al., The impact of age on outcome of embryonal and alveolar rhabdomyosarcoma patients. A multicenter study, Anticancer Res 32 (10) (2012) 4485–4497.
[11] A. Ferrari, M. Casanova, G. Bisogno, et al., Rhabdomyosarcoma in infants younger than one year old, Cancer 97 (10) (2003) 2597–2604, https://doi.org/10.1002/cncr.11357.
[12] J.L. Meza, J. Anderson, A.S. Pappo, W.H. Meyer, Analysis of prognostic factors in patients with nonmetastatic rhabdomyosarcoma treated on intergroup rhabdomyosarcoma studies III and IV: The Children's Oncology Group, J. Clin. Oncol. 24 (24) (2006) 3844–3851, https://doi.org/10.1200/JCO.2005.05.3801.
[13] T. Butel, M. Karanian, G. Pierron, et al., Integrative clinical and biopathology analyses to understand the clinical heterogeneity of infantile rhabdomyosarcoma: a report from the French MMT committee, Cancer Med. 9 (8) (2020) 2698–2709, https://doi.org/10.1002/cam4.2713.
[14] A.A. Gupta, J.R. Anderson, A.S. Pappo, et al., Patterns of chemotherapy-induced toxicities in younger children and adolescents with Rhabdomyosarcoma: a report from the children's oncology group soft tissue sarcoma committee, Cancer 118 (4) (2012) 1130–1137, https://doi.org/10.1002/cncr.26358.
[15] S. Patrizi, E. Miele, L. Falcone, et al., Malignant peripheral nerve sheath tumor (MPNST) and MPNST-like entities are defined by a specific DNA methylation

profile in pediatric and juvenile population, Clin. Epigenet. 16 (2024) 9, https://doi.org/10.1186/s13148-023-01621-7.
[16] Z.L. Skidmore, A.H. Wagner, R. Lesurf, et al., GenVisR: genomic visualizations in R, Bioinformatics 32 (19) (2016) 3012–3014, https://doi.org/10.1093/bioinformatics/btw325.
[17] Y. Tian, T.J. Morris, A.P. Webster, et al., ChAMP: updated methylation analysis pipeline for Illumina BeadChips, Bioinformatics 33 (24) (2017) 3982–3984, https://doi.org/10.1093/bioinformatics/btx513.
[18] C. Koelsche, D. Schrimpf, D. Stichel, et al., Sarcoma classification by DNA methylation profiling, Nat. Commun. 12 (2021) 498, https://doi.org/10.1038/s41467-020-20603-4.
[19] A.E. Teschendorff, F. Marabita, M. Lechner, et al., A beta-mixture quantile normalization method for correcting probe design bias in Illumina Infinium 450 k DNA methylation data, Bioinformatics 29 (2) (2013) 189–196, https://doi.org/10.1093/bioinformatics/bts680.
[20] A.E. Teschendorff, A comparison of epigenetic mitotic-like clocks for cancer risk prediction, Genome Med. 12 (1) (2020) 56, https://doi.org/10.1186/s13073-020-00752-3.
[21] S. Chen, Y. Zhou, Y. Chen, J. Gu, fastp: an ultra-fast all-in-one FASTQ preprocessor, Bioinformatics 34 (17) (2018) i884–i890, https://doi.org/10.1093/bioinformatics/bty560.
[22] A. Dobin, C.A. Davis, F. Schlesinger, et al., STAR: ultrafast universal RNA-seq aligner, Bioinforma. Oxf. Engl. 29 (1) (2013) 15–21, https://doi.org/10.1093/bioinformatics/bts635.
[23] S. Uhrig, J. Ellermann, T. Walther, et al., Accurate and efficient detection of gene fusions from RNA sequencing data, Genome Res 31 (3) (2021) 448–460, https://doi.org/10.1101/gr.257246.119.
[24] Nicorici D., Şatalan M., Edgren H., et al. FusionCatcher – a tool for finding somatic fusion genes in paired-end RNA-sequencing data. Published online November 19, 2014:011650. doi:10.1101/011650.
[25] E. Guadagnin, P. Mohassel, K.R. Johnson, et al., Transcriptome analysis of collagen VI-related muscular dystrophy muscle biopsies, Ann. Clin. Transl. Neurol. 8 (11) (2021) 2184–2198, https://doi.org/10.1002/acn3.51450.
[26] R. Patro, G. Duggal, M.I. Love, R.A. Irizarry, C. Kingsford, Salmon: fast and bias-aware quantification of transcript expression using dual-phase inference, Nat. Methods 14 (4) (2017) 417–419, https://doi.org/10.1038/nmeth.4197.
[27] Love M.I., Soneson C., Hickey P.F., et al. Tximeta: reference sequence checksums for provenance identification in RNA-seq. Published online September 25, 2019: 777888. doi:10.1101/777888.
[28] M.I. Love, W. Huber, S. Anders, Moderated estimation of fold change and dispersion for RNA-seq data with DESeq2, Genome Biol. 15 (12) (2014) 550, https://doi.org/10.1186/s13059-014-0550-8.
[29] I.R. Lanza, D.K. Short, K.R. Short, et al., Endurance exercise as a countermeasure for aging, Diabetes 57 (11) (2008) 2933–2942, https://doi.org/10.2337/db08-0349.
[30] M. Cassandri, R. Fioravanti, S. Pomella, et al., CDK9 as a valuable target in cancer: from natural compounds inhibitors to current treatment in pediatric soft tissue sarcomas, Front. Pharm. 11 (2020), https://doi.org/10.3389/fphar.2020.01230.
[31] B.E. Gryder, M.E. Yohe, H.C. Chou, et al., PAX3-FOXO1 establishes myogenic super enhancers and confers BET bromodomain vulnerability, Cancer Discov. 7 (8) (2017) 884–899, https://doi.org/10.1158/2159-8290.CD-16-1297.
[32] J.H. Turner, J.D. Richmon, Head and neck rhabdomyosarcoma: a critical analysis of population-based incidence and survival data, Otolaryngol. Neck Surg. 145 (6) (2011) 967–973, https://doi.org/10.1177/0194599811417063.
[33] M. Jothi, K. Nishijo, C. Keller, A.K. Mal, AKT and PAX3-FKHR cooperation enforces myogenic differentiation blockade in alveolar rhabdomyosarcoma cell, Cell Cycle 11 (5) (2012) 895–908, https://doi.org/10.4161/cc.11.5.19346.
[34] S. Ramírez-Peinado, F. Alcázar-Limones, L. Lagares-Tena, et al., 2-deoxyglucose induces noxa-dependent apoptosis in alveolar rhabdomyosarcoma, Cancer Res. 71 (21) (2011) 6796–6806, https://doi.org/10.1158/0008-5472.CAN-11-0759.
[35] A.G. Jacob, D. O'Brien, R.K. Singh, et al., Stress-induced isoforms of MDM2 and MDM4 correlate with high-grade disease and an altered splicing network in pediatric rhabdomyosarcoma, Neoplasia N. Y N. 15 (9) (2013) 1049–1063.
[36] G. Rammal, A. Fahs, F. Kobeissy, et al., Proteomic profiling of rhabdomyosarcoma-derived exosomes yield insights into their functional role in paracrine signaling, J. Proteome Res 18 (10) (2019) 3567–3579, https://doi.org/10.1021/acs.jproteome.9b00157.
[37] W.E. Hathaway, T. Hays, Hypercoagulability in childhood cancer, J. Pedia Surg. 10 (6) (1975) 893–899, https://doi.org/10.1016/S0022-3468(75)80092-3.
[38] S. Sallah, J.Y. Wan, N.P. Nguyen, L.R. Hanrahan, G. Sigounas, Disseminated intravascular coagulation in solid tumors: clinical and pathologic study, Thromb. Haemost. 86 (3) (2001) 828–833.
[39] C. De Giovanni, L. Landuzzi, A. Palladini, G. Nicoletti, P. Nanni, P.L. Lollini, HER tyrosine kinase family and rhabdomyosarcoma: role in onset and targeted therapy, Cells 10 (7) (2021) 1808, https://doi.org/10.3390/cells10071808.
[40] R.L. Walker, F.J. Hornicek, Z. Duan, Transcriptional regulation and therapeutic potential of cyclin-dependent kinase 9 (CDK9) in sarcoma, Biochem. Pharm. 226 (2024) 116342, https://doi.org/10.1016/j.bcp.2024.116342.
[41] R. Mandal, S. Becker, K. Strebhardt, Targeting CDK9 for anti-cancer therapeutics, Cancers 13 (9) (2021) 2181, https://doi.org/10.3390/cancers13092181.
[42] G. H.S. Richter, T. Hensel, O. Schmidt, et al., Combined inhibition of epigenetic readers and transcription initiation targets the EWS-ETS transcriptional program in Ewing Sarcoma, Cancers 12 (2) (2020) 304, https://doi.org/10.3390/cancers12020304.
[43] Sellas Life Sciences Group. A Phase I/IIa, Open-Label Dose Escalation and Dose Expansion Study of Intravenous GFH009 Single Agent and in Combination With Venetoclax and Azacitidine in Patients With Relapsed/Refractory Hematologic Malignancies. clinicaltrials.gov; 2024. Accessed February 3, 2025. ⟨https://clinicaltrials.gov/study/NCT04588922⟩.
[44] Cyclacel Pharmaceuticals, Inc. A Phase 1/2, Open-Label, Multicenter Study to Investigate the Safety, Pharmacokinetics, and Efficacy of Fadraciclib (CYC065), an Oral CDK9 Inhibitor, in Subjects With Advanced Solid Tumors and Lymphoma. clinicaltrials.gov; 2024. Accessed February 3, 2025. ⟨https://clinicaltrials.gov/study/NCT04983810⟩.
[45] O. Slater, J.E. Gains, A.M. Kelsey, et al., Localised rhabdomyosarcoma in infants (<12 months) and young children (12–36 months of age) treated on the EpSSG RMS 2005 study, Eur. J. Cancer 160 (2022) 206–214, https://doi.org/10.1016/j.ejca.2021.10.031.